

# Velocity-field characteristics of III-V semiconductor alloys: Band structure influences

Srinivasan Krishnamurthy and A. Sher

Physical Electronics Laboratory, SRI International, Menlo Park, California 94025

A.-B. Chen

Department of Physics, Auburn University, Auburn, Alabama 36801

(Received 30 May 1986; accepted for publication 31 October 1986)

We have calculated the velocity-field characteristics of semiconductor alloys based on realistic band structures and have obtained the band structures and alloy-scattering rates from a generalization of the coherent potential approximation method. Although we use proper band structures, we still consider a single electron-temperature model. The results agree surprisingly well with experiments, and suggest that InP-based alloys are good candidates for high-speed devices.

## I. INTRODUCTION

The electron drift velocity  $v$ , in many semiconductors, increases nonlinearly under the influence of high applied electric field to reach a peak value  $v_p$  at a threshold field  $E_T$ ; any further increase of  $E$  results in reduced  $v$ , giving rise to a negative differential resistance. High-speed device applications benefit from materials with maximum  $v_p$  and minimum  $E_T$ . In this paper, we examine the influence of the alloy composition variation of the band structures on velocity-field characteristics of several III-V ternary alloys. In the past,  $v$ - $E$  characteristics<sup>1-3</sup> have been calculated in a variety of approximations. In simplest two-valley models, each valley is characterized by a different effective mass. Their minima are separated by an offset energy,  $\Delta E$ ; these three parameters, along with electron-phonon coupling constants, are adjusted to fit the observed  $v$ - $E$  curves. In more elaborate approximations, the central and satellite valley masses are calculated from  $k \cdot p$  theory,  $\Delta E$  is determined from optical experiments, and the electron-phonon coupling constants are calculated. By contrast, all of these quantities are calculated from a full band structure theory.

The effect of alloy scattering on low field mobility has been evaluated by various authors.<sup>4-6</sup> The main difficulty in extending these models to the hot-electron problem is in applying an appropriate correction for the change in effective mass and scattering potential with wave vector  $k$ . Also, the effect of scattering depends on what model is chosen to evaluate the scattering potential.<sup>2</sup> Our improvement over previous efforts is to use accurate alloy band structures and scattering rates for many systems. The most general  $v$ - $E$  results are calculated in a strong-multiple-scattering formalism known as the *coherent potential approximation* (CPA), where the alloy scattering rate is calculated directly from an imaginary part of the self-energy. In this formalism, the non-parabolic, anisotropic, and intervalley scattering mediated by alloy disorder is included without adjustable parameters. Our aim is to examine systematically the factors that limit the values of  $E_T$  and  $v_p$ , and thereby to suggest likely materials for high-speed device applications.

## II. MODEL FOR $v$ - $E$ CHARACTERISTICS

Many numerical methods available in the literature<sup>7-10</sup> lead to approximate solutions to the Boltzmann equation. The *iterative* approach<sup>8</sup> combined with the Monte Carlo technique has been widely used to study hot-electron problems.<sup>3,11</sup> While hot-electron distributions calculated from Monte Carlo solutions to the Boltzmann equation may be more accurate for the present study (which is designed to compare the merits of many materials), we have adopted a simple hot-electron theory<sup>2</sup> that assumes a "drifted Maxwellian" electron distribution with a single electron temperature  $T_e$ . Such a distribution would be established only if some interaction (e.g., like electron-electron scattering) were to drive the electron system into internal equilibrium at a rate fast compared to the rate of energy exchange with the heat bath.<sup>12</sup> No such interaction has ever been identified; for example, Coulomb-coupled electron-electron interactions require a much higher electron density than what is actually used in devices to achieve sufficiently high scattering rates that the electron temperature conditions are satisfied. Nevertheless, as we shall demonstrate, the predictions based on a drifted Maxwellian distribution are surprisingly accurate, and thus serve as a good vehicle for this systematic study.

Under high-field conditions, the electrons gain energy when they are accelerated from the conduction-band minimum to higher energy levels. The average electron energy in steady state is often considerably higher than the average lattice excitation energy per particle. The electron temperature  $T_e$ , which reflects the average electron energy, is therefore much higher than the lattice temperature  $T$ . For all direct-gap semiconductors considered here, the mobility in the lower valley, denoted  $\mu_1$ , is much larger than that in the higher valleys, denoted  $\mu_2$ . Assuming  $\mu_2 \cong 0$ , the drift velocity can be approximated by<sup>2</sup>

$$v = \mu_1 E / (1 + R e^{-\Delta E / kT_e}), \quad (1)$$

where  $R$  is the ratio between the densities of states in the upper and lower valleys, respectively, and  $\Delta E$  is the energy difference between the minima of these two valleys. In

steady state, the energy gained by an electron from the field must be balanced by the energy lost to the lattice:

$$evE = \frac{3}{2} k(T_e - T)/\tau_E, \quad (2)$$

where  $\tau_E$  is the electron-lattice energy relaxation time. Equations (1) and (2) combine to yield  $T_e$ , which in turn yields the  $v$ - $E$  characteristic curve and hence the threshold values  $E_T$  and  $v_p$ . These values have the approximate forms  $v_p \propto \sqrt{\mu_1 \Delta E / \tau_E}$  and  $E_T \propto \sqrt{R \Delta E / \mu_1 \tau_E}$ .

Alloy effects come not only from the concentration dependence of the band parameters  $R$  and  $\Delta E$ , but also from the effect of alloy scattering on the mobility. We take  $\mu_1$  to be

$$\mu_1^{-1} = \mu_0^{-1}(T) + \mu_A^{-1}(T_e),$$

where  $\mu_0$  is the mobility limited by all scattering mechanisms *except* alloy scattering and is taken as the concentration-weighted average of the experimental values of the two constituent compounds.  $\mu_A$  is the alloy-scattering-limited mobility and is calculated using a generalized Brooks' formula.<sup>6</sup>

Finally, we assume that electrons lose energy at the lattice mainly through polar optical phonon scattering and calculate  $\tau_E$  from Eq. (3.6.26) of Ref. 1. The electron and lattice parameters needed for this estimate are all taken to be the concentration-weighted averages of the pure crystal constituents.

### III. BAND STRUCTURES

To calculate the alloys' band structures, we must begin with those of the pure compounds. We have demonstrated<sup>13</sup> that quantitatively accurate band structures for II-VI and III-V compounds can be obtained using a minimum set of four  $sp^3$  Slater orbitals per atom in a semiempirical calculation. First, the empirical pseudopotential form factors are used to construct a tight-binding (TB) Hamiltonian  $H$  in this minimum set.  $H$  is then transformed into a zeroth order  $H_0$  in an orthonormal basis. Then a perturbative Hamiltonian having a first-neighbor TB form and a site-diagonal spin-orbit Hamiltonian are added to obtain a fine-tuned band structure. This band structure accurately reproduces the energy separation between the lowest and the next lowest minima in the conduction bands, the band gap  $E_g$ , and the conduction-band effective mass  $m^*$ .

Figure 1 shows an example of a band structure for InAs. A detailed comparison of the symmetry point energies and effective masses to experimental values reveals that the accuracy of our band structures is comparable to the best available.<sup>14</sup> The band structure obtained in this way is superior to the results of the usual first- or second-neighbor TB approach, because our method includes all the long-range interactions. Figures 2(a) and (b) show the lowest conduction band in  $\Gamma X$  and  $\Gamma L$  directions for InAs, InSb, InP and GaAs, GaSb compounds, respectively. The phenomena we are examining are only sensitive to energy variation of states relative to the conduction minima; accordingly, we have drawn all the curves with their conduction-band edges aligned. Because the InP, InSb conduction bands cross in Fig. 2(a), their alloys will have larger  $\mu_1$  but smaller  $\Delta E$  than does InP. The peak velocity in these alloys can be larger than that of InP. However, both  $\mu_1$  and  $\Delta E$  will be larger in

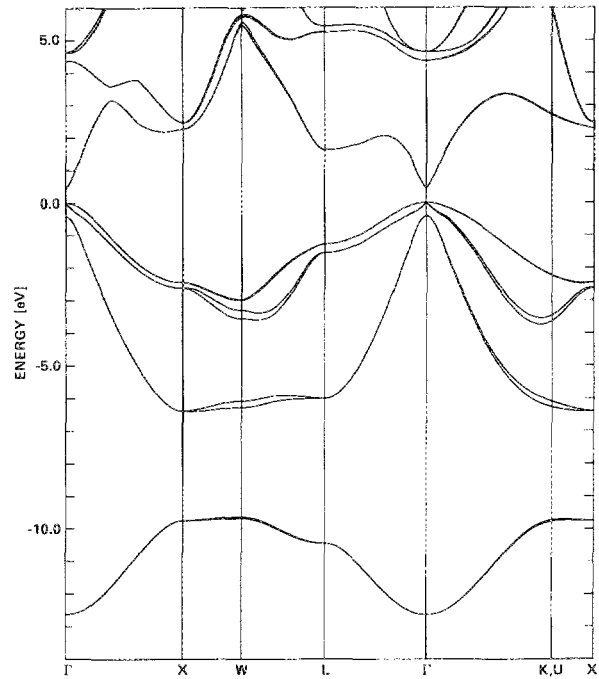


FIG. 1. Band structure of InAs. Energy in eV.

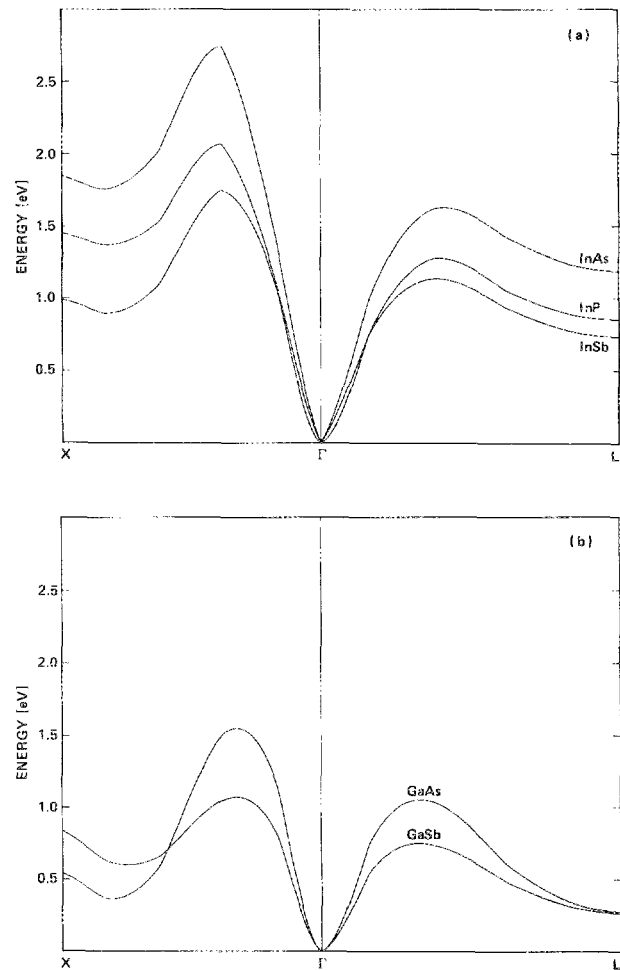


FIG. 2. Lowest conduction band of (a) InP, InAs, InSb, and (b) GaAs, GaSb compounds. All energies measured in eV with respect to their respective conduction-band minima.

InPAs alloys than that in InP; and, thus, one can expect a moderate increase in  $v_p$  and  $E_T^{-1}$ . In GaAs and GaSb,  $\mu_1$  and  $\Delta E$  are almost the same. Hence, electron-phonon interactions will dominate the change in  $v$ - $E$  characteristics.

Table I lists the important band parameters of the five pure III-V compounds included in this study. Also listed are the minimum energies  $E_p$  at which a hot electron can create an electron-hole pair;  $E_p$  is given by  $E_g [(1 + 2\alpha)/(1 + \alpha)]$ , where  $\alpha$  is the ratio of the electron mass to the heavy-hole mass.<sup>15</sup> The values for these pure-crystal band structures are the input to the alloy electronic structure calculation using the CPA.<sup>13</sup> Both diagonal disorder (due to atomic term value differences) and off-diagonal disorder (due to bond-length fluctuations) are treated. The method is a generalization of the tight-binding "molecular CPA" of Hass *et al.*<sup>16</sup> to our better band structures. From the CPA self-energy, one can obtain the alloy band gap,  $m^*$ ,  $\Delta E$ ,  $R$ , and  $\mu_1$  as a function of the alloy concentration  $x$ . These quantities are then used to calculate the  $v$ - $E$  characteristics, as we described in Sec. II.

#### IV. EXAMPLE: Ga<sub>x</sub>In<sub>1-x</sub>As

As an example, we present here in some detail the results of our calculations for Ga<sub>x</sub>In<sub>1-x</sub>As. Figure 3 contains plots of  $\Delta E$ ,  $E_p$  ( $\cong E_g$ ), and  $v_p$  at two temperatures as a function of  $x$ . If  $\Delta E$  is larger than  $E_p$ , avalanche breakdown is expected to occur before  $v_p$  is reached. Thus, the velocity-field plot near  $v_p$  is only meaningful for the range of  $x$  where  $\Delta E < E_p$ . The maximum value of  $v_p$  that can be obtained for this alloy is at  $x \cong 0.47$ . The peak velocity  $v_p$  is seen to be a nonlinear function of  $x$ . Experimental<sup>17</sup> values of  $v_p$  (open circle) are also plotted.

Because we set the mobility of the satellite valley equal to zero in Eq. (1), we should not expect the model to be accurate for electric fields much higher than  $E_T$ . Nevertheless, it is interesting to examine the  $v$ - $E$  curves shown in Fig. 4 produced by the model at room temperature and the different  $x$  values. Because the mobility of InAs is larger than that of GaAs, the slope in the low field region decreases with  $x$ . For the same reason,  $E_T$  increases with  $x$ . This prediction of a larger  $v_p$  value and a smaller  $E_T$  at lower GaAs content has been observed experimentally.<sup>11</sup> At  $x = 0.47$ , the  $v_p$  value is about 50% larger than that of GaAs, once again in agreement with experiments.<sup>17,18</sup>

The effect of the lattice temperature on the  $v$ - $E$  characteristics is illustrated in Fig. 5. The curve sharpens at low  $T$ , and the  $v_p$  value increases because both  $\mu_0$  and  $\mu_A$  are larger at lower  $T$ .

TABLE I. Important band parameters of III-V compounds.

Parameter	GaAs	InAs	InP	GaSb	InSb
$E_g$ (eV)	1.52	0.42	1.42	0.86	0.25
$m^*$ ( $m_0$ )	0.067	0.026	0.072	0.050	0.018
$\Delta E$ (eV)	0.282	1.11	0.82	0.27	0.73
$R$	42.95	186.02	45.02	200.10	1493.14
$E_p$ (eV)	1.70	0.44	1.54	0.98	1.26

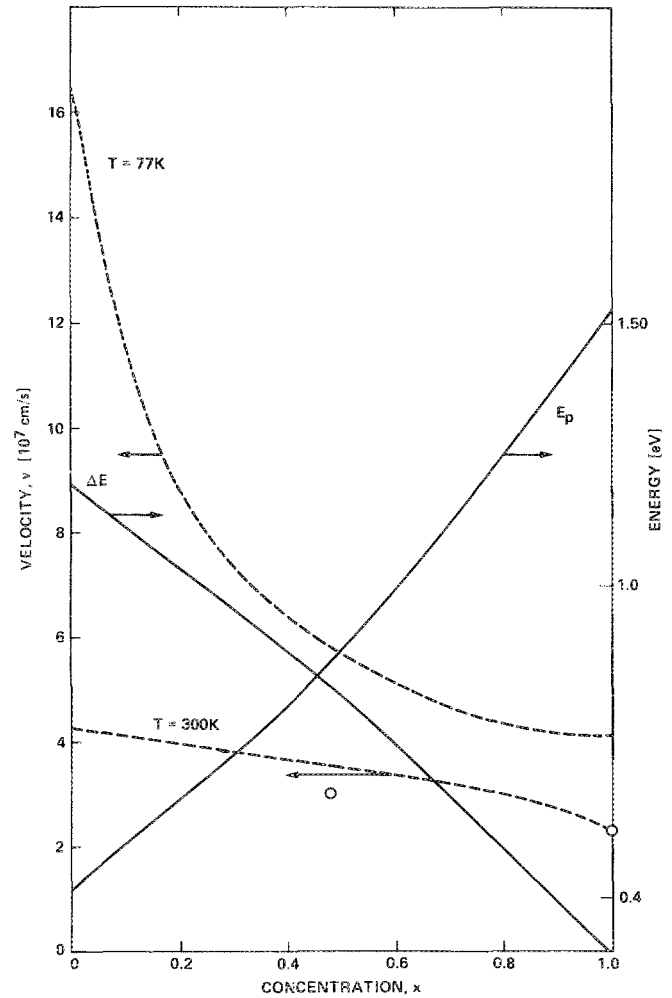


FIG. 3. Variation of  $\Delta E$ ,  $E_p$ ,  $v_p$  as a function of GaAs concentration,  $x$  in Ga<sub>x</sub>In<sub>1-x</sub>As alloys. Experimental values (open circle) of  $v_p$  are from Ref. 11.

Figure 6 depicts two effects: the influence of alloy scattering on the  $v$ - $E$  characteristics and the errors caused by the effective mass approximation (EMA). All three curves are for  $x = 0.5$  and a  $T = 300$  K. Curve (a) does not include alloy scattering and curve (c) does, but both are based on EMA. Because the presence of alloy scattering reduces the effective mobility, curve (c) starts with a smaller slope and has a smaller  $v_p$  and a long tail as it approaches  $v_p$ , causing its  $E_T$  to be larger than curve (a). The reduction of  $v_p$  by alloy scattering in this case is about 30%. Curve (b) represents the results of a more detailed calculation using the actual density of states (DOS). Instead of Eq. (1), the drift velocity in this calculation is obtained from  $v = \sigma E / (ne)$ , where  $n$  is the electron density and  $\sigma$  is given by

$$\sigma = \frac{2}{3} e^2 \int v^2(\epsilon) \tau(\epsilon) \left( \frac{-\partial f}{\partial \epsilon} \right) d\epsilon, \quad (3)$$

with  $\tau(\epsilon)$  being the average momentum collision time,  $f$  the electron distribution, and  $v^2$  the energy-shell average of the square of the group velocity

$$v^2(\epsilon) = \sum_{nk} |\mathbf{v}_n(k)|^2 \delta[\epsilon - \epsilon_n(k)]. \quad (4)$$

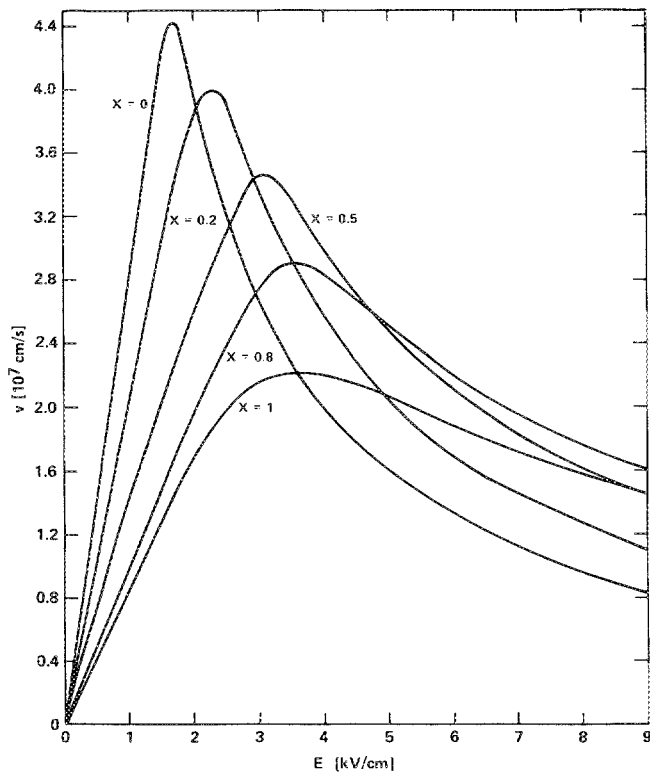


FIG. 4. Velocity-field characteristics of  $\text{Ga}_x \text{In}_{1-x} \text{As}$  alloys.

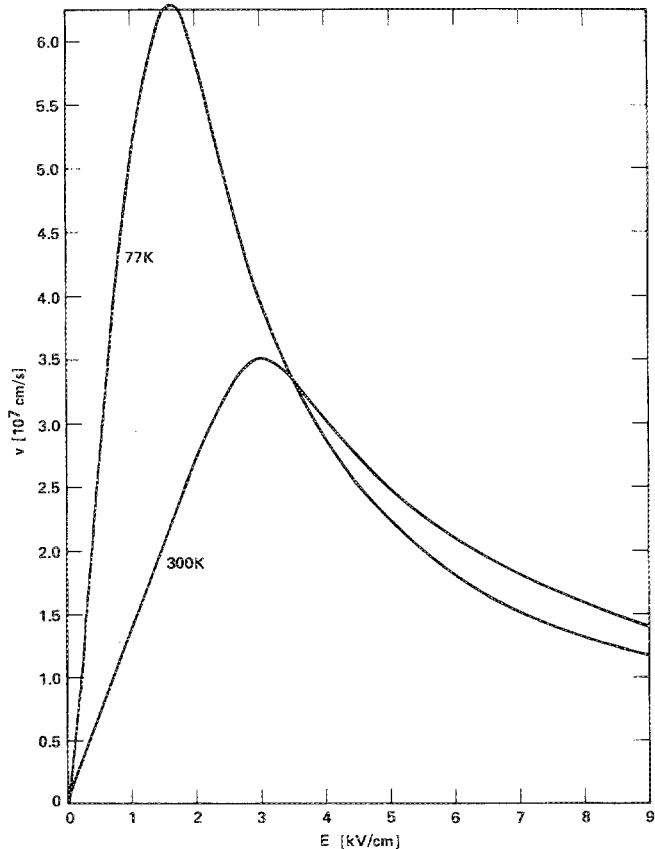


FIG. 5. Temperature dependence of  $v$ - $E$  characteristics of  $\text{Ga}_{0.5} \text{In}_{0.5} \text{As}$  alloy.

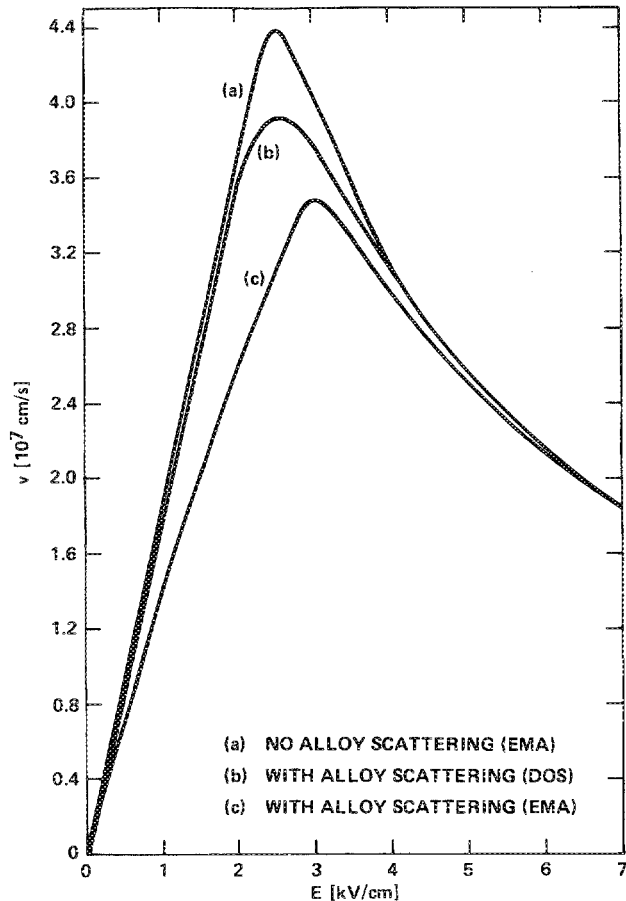


FIG. 6. Effect of band structure and alloy scattering on  $v$ - $E$  characteristics for  $\text{Ga}_{0.5} \text{In}_{0.5} \text{As}$  at 300 K. Results of the calculations (a) in EMA without alloy scattering, (b) in EMA with alloy scattering, and (c) with exact DOS and alloy scattering.

Thus, curve (b) does not assume a zero mobility for the higher valleys as was assumed in curves (a) and (c). We, therefore, infer that the effective mobility in curve (b) lies between those of curves (a) and (c). Comparison between curves (b) and (c) shows that the more elaborate calculation tends to predict a moderate increase in  $v_p$  and a small reduction in  $E_T$ , largely because the bands increase with  $k$  more rapidly than quadratically before they bend over toward the satellite valley. Thus, the effective mass as a function of  $k$ , actually first becomes smaller, then larger until the inflection point is reached; thereafter, the curvature changes sign and the effective mass becomes negative. The alloy mobility varies roughly as  $(m^*)^{-5/2}$ , so the net effect of the smaller  $m^*$  in the critical region is to produce curve (b). Moreover, the real part of the alloy scattering self-energy must also play a role, because it too modifies the energy bands. Thus, Monte Carlo calculations (which treat scattering on fixed energy band structures) cannot be expected to reproduce the same numerical result and in this instance are therefore less accurate than the CPA results.

#### V. OTHER TERNARY ALLOYS

We have carried out the calculations described above for the direct-gap ternary alloys  $\text{GaInSb}$ ,  $\text{InAsP}$ ,  $\text{InAsSb}$ ,  $\text{GaAsSb}$ , and  $\text{InPSb}$ . The results are summarized in Fig. 7,

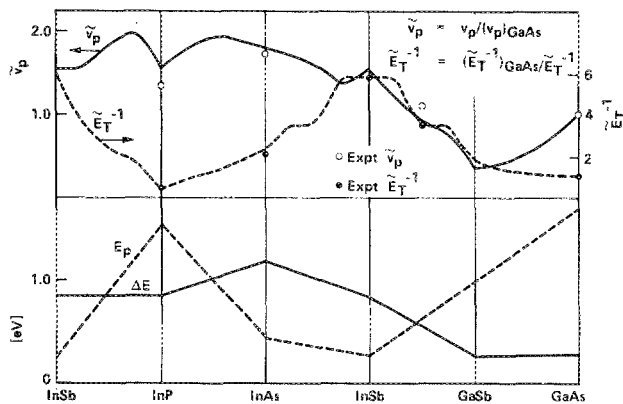


FIG. 7. Variations of  $\Delta E$  (solid line—in lower half),  $E_p$  (dotted line—in lower half),  $\tilde{v}_p$  (solid line—in upper half), and  $\tilde{E}_T^{-1}$  (dotted line—in upper half) are shown.  $\tilde{v}_p$ ,  $\tilde{E}_T^{-1}$  are peak velocity and threshold field in the unit of respective GaAs values. The experimental values of peak velocity (open circles) and threshold fields (filled circles) are also shown.

where we plot the values of  $\tilde{v}_p$  and  $\tilde{E}_T^{-1}$ , which are, respectively, the  $v_p$  and  $E_T^{-1}$  normalized to GaAs values. Values of  $\Delta E$  and  $E_p$  are also plotted. Only for those few alloys satisfying the condition  $E_p > \Delta E$  can the peak values,  $v_p$ , shown actually be reached before avalanche breakdown takes place. The circles are the available experimental values<sup>17,18</sup> for  $v_p$ . Considering the simplifications involved in the model, the agreement with experiment is remarkable.

It is interesting to note that  $\tilde{v}_p$  is greater in InPSb than in pure InP and InSb, although alloy scattering tends to reduce  $\tilde{v}_p$ . Similar results are also seen in the InPAs alloy. These results can be explained as follows: The phonon-driven energy-exchange rate with the electrons in InP is larger than that in either InSb or InAs. However, because of the larger electron effective mass, the mobility in InP is much smaller than those in InSb or InAs. The combined effect gives rise to a larger  $v_p$  for the alloys. The ratio of the peak velocity to the energy dissipated by an electron traveling at this velocity is  $E_T^{-1}$ ; accordingly,  $\tilde{E}_T^{-1}$  measures the efficiency of an alloy relative to GaAs in high-speed device applications. Our calculation of  $\tilde{E}_T^{-1}$  also agrees very well with the available experimental data.

## VI. SUMMARY

We have carried out a comparative evaluation of the influence of band structure features of several III-V compound alloys on velocity-field characteristics using detailed band structures and alloy scattering rates. Our results suggest that InP-based alloys are even more promising candidates for high-speed devices than GaAs. A more rigorous study is in progress to improve the accuracy of our calculations and further check this prediction.

## ACKNOWLEDGMENT

This work was supported by DARPA Contract F49620-85-C-0103.

- <sup>1</sup>E. M. Conwell, *Solid State Physics*, Vol. 9 (Academic, New York, 1967) and references cited therein.
- <sup>2</sup>S. M. Sze, *Physics of Semiconductor Devices* (Wiley, New York, 1978), p. 645, and references cited therein.
- <sup>3</sup>J. R. Hauser, M. A. Littlejohn, and T. H. Glisson, *Appl. Phys. Lett.* **28**, 458 (1976).
- <sup>4</sup>L. Makowski and M. Glicksman, *J. Phys. Chem. Solids* **34**, 487 (1973).
- <sup>5</sup>M. A. Littlejohn, J. R. Hauser, T. H. Glisson, D. K. Ferry, and J. W. Harrison, *Solid State Electron* **21**, 107 (1978).
- <sup>6</sup>S. Krishnamurthy, A. Sher, and A.-B. Chen, *Appl. Phys. Lett.* **47**, 160 (1985).
- <sup>7</sup>T. Kurosawa, *Proceedings of the International Conference Physics of Semiconductors*, Kyoto, *J. Phys. Soc. Jpn. (suppl)* **21**, 424 (1966).
- <sup>8</sup>H. D. Rees, *J. Phys. Chem. Solids* **30**, 643 (1969).
- <sup>9</sup>C. Hammar, *J. Phys. C* **6**, 70 (1973).
- <sup>10</sup>P. J. Price, *Solid State Electron* **21**, 9 (1978).
- <sup>11</sup>B. R. Nag, *Pramāna* **23**, 411 (1984).
- <sup>12</sup>A. Sher and H. Primakoff, *Phys. Rev.* **130**, 1267 (1963).
- <sup>13</sup>A.-B. Chen and A. Sher, *Phys. Rev. B* **23**, 5360 (1981).
- <sup>14</sup>J. R. Chelikowsky and M. L. Cohen, *Phys. Rev. B* **14**, 556 (1976) and references cited therein.
- <sup>15</sup>*Handbook of Physics*, 3rd Ed. (McGraw-Hill, New York, 1972).
- <sup>16</sup>K. C. Hass, R. J. Lampart, and H. Ehrenreich, *Phys. Rev. Lett.* **52**, 77 (1984).
- <sup>17</sup>T. H. Windhorn, L. W. Cook, and G. E. Stillman, *J. Elec. Mater.* **11**, 1065 (1982); *IEEE Electron. Devices Lett.* **EDL-3**, 18 (1982).
- <sup>18</sup>W. Kowalsky and A. Schlacketzki, *Solid State Electron.* **28**, 299 (1985).